HIGH RESOLUTION RADAR IMAGING

Semi-Annual Progress Report
O.N.R. Contract N00014-86-K-0370
Period: 1 June 1988–30 November 1988

Principal Investigator: Donald L. Snyder

Washington
WASHINGTON·UNIVERSITY·IN·ST·LOUIS

ELECTRONIC SYSTEMS AND SIGNALS RESEARCH LABORATORY

Department of Electrical Engineering
Campus Box 1127
One Brookings Drive
Washington University

HIGH RESOLUTION RADAR IMAGING

Semi-Annual Progress Report No. 5

Office of Naval Research Contract Number N00014-86-K-0370

Period Covered: 1 June 1988 - 30 November 1988

Principal Investigator:

Donald L. Snyder
Director, Electronic Systems and Signals Research Laboratory
Washington University
Campus Box 1127
One Brookings Drive
St. Louis, Missouri 63130

Scientific Program Director:

Dr. Rabinder Madan
Office of Naval Research
Code 1114SE
800 North Quincy Street
Arlington, Virginia 22217-5000

DISTRIBUTION

	copies
Mr. John W. Michalski Office of Naval Research Resident Representative Federal Building, Room 286 536 South Clark Street Chicago, Illinois 60605-1588	1
Dr. Rabinder N. Madan Office of Naval Research 800 N. Quincy Street Code 1114SE Arlington, Virginia 22217-5000	1
Director Naval Research Laboratory Attn.: Code 2627 Washington, DC 20375	1
Defense Technical Information Center Building 5 Cameron Station Alexandria, Virginia 22314	12
Mr. Harper J. Whitehouse Naval Ocean Systems Center Code 7402 San Diego, California 92152	1
Dr. James Fienup Environmental Research Institute of Michigan P.O. Box 8618 Ann Arbor, MI 48107	1
Dr. Kenneth Senne M.I.T. Lincoln Laboratory Lexington, MA 02173	1
Dr. Richard E. Blahut I.B.M. Owego, New York 13827	1

Table of Contents

1. Introduction

This semi-annual progress report contains a summary of work accomplished on O. N. R. contract number N00014-86-K-0370, *High Resolution Radar Imaging*, during the period from 1 June 1988 to 30 November 1988.

The goal of this project is to formulate and investigate new approaches for forming images of radar targets from spotlight-mode, delay-doppler measurements. These measurements could be acquired with a high-resolution radar-imaging system operating with an optical- or radio-frequency carrier. Two approaches are under study. The first is motivated by an image-reconstruction algorithm used in radionuclide imaging called the *confidence-weighted algorithm*; here, we will refer to this approach as the *chirp-rate modulation approach*. The second approach is based on more fundamental principles which starts with a mathematical model that accurately describes the physics of an imaging radar-system and then uses statistical-estimation theory with this model to derive processing algorithms; we will refer to this as the *estimation-theory approach*.

Work accomplished during the reporting period is summarized in the following section.

2. Summary of Work Accomplished

Progress during this reporting period has been made on: a, extending the estimation-theory approach to include a constraint on input signal-to-noise ratio; b, extending the estimation-theory approach to include a sieve constraint for stabilizing image estimates; c, extending the estimation-theory approach to include a specular or glint component in the radar-echo data; d, analyzing the performance of the estimation-theory approach through computer simulations; and e, modifying the chirp-rate modulation approach through the introduction of the Wigner-Ville distribution. Some of these areas are described briefly below and more completely in the appendices. A patent was awarded associated with the chirp-rate modulation approach.

2.1. Estimation-Theory Approach to Imaging

During this reporting period, a major effort has been expended in implementing and conducting computer simulations to evaluate the performance of this imaging approach compared to the conventional appraoch based on Fourier transforms. Preliminary results are reported in reference

[1], a preprint of which is included in Appendix 1. We have extended the estimation-theory approach to include constraints on the input signal-to-noise ratio and for including sieve constraints to stabilize estimated target images. We have found that such constraints can improve the performance significantly, as described briefly in [1] for the SNR constraint. A simulation program is presently being prepared to run equations of the estimation-theory approach on an Active Memory Technology Distributed Array Processor having 1024 processors connected in a mesh array; we expect that this will permit us to perform simulations with modest sized images for performance evaluation studies. Effort continued to extend our model to include specular components in the return signal; a brief status report is contained in Appendix 2.

2.2. Chirp-Rate Modulation Approach to Imaging

A patent was issued jointly to H. J. Whitehouse, of the Naval Ocean Systems Center in San Diego, and D. L. Snyder for the chirp-rate modulation approach to imaging based on the use of the confidence-weighted algorithm [2]. A copy of this is in Appendix 3.

The focus of our research on the chirp-rate modulation approach during the reporting period has been on modifying the image formation equations following the introduction of the use of the Wigner-Ville distribution into the problem by H. Whitehouse [3].

3. References

1. P. Moulin, D. L. Snyder, and J. A. O'Sullivan, "Maximum-Likelihood Spectrum Estimation of Periodic Processes from Noisy Data," submitted for presentation at the 1989 Conference on Information Sciences and Systems, Johns Hopkins University, March 1989. A preprint is in Appendix 1.

2. H. J. Whitehouse and D. L. Snyder, *Imaging System*, U.S. Patent Number 4,768,156, Aug. 30, 1988. A preprint is in Appendix 2.

3. H. J. Whitehouse, "Delay-Doppler Radar/Sonar Imaging," presented at the Summer Program on Signal Processing, Institute of Mathematics and Its Applications, Univ. of Minnesota, Minneapolis, Aug. 1988.

4. Appendices

4.1. Appendix 1. Preprint of Reference [1].

Maximum-Likelihood Spectrum Estimation of Periodic Processes from Noisy Data *

P. Moulin
D. L. Snyder
J. A. O'Sullivan

Electronic Systems and Signals Research Laboratory
Department of Electrical Engineering
Washington University
Saint Louis, MO 63130

ABSTRACT

We have developed a new approach to maximum-likelihood spectrum estimation of wide-sense stationary processes from noisy data. A statistical model for the data is defined: The process whose spectrum is sought is wide-sense stationary, periodic and Gaussian, and its observations are corrupted by an additive white noise. A maximum-likelihood formulation of this problem has been derived, and the equations are solved numerically via the expectation-maximization algorithm. This approach presents several attractive features, an important one being that the noise corrupting the observations is now taken into account.

We present some recent developments for this problem. The statistical performance of the new maximum-likelihood spectrum estimator is studied both theoretically and numerically. Comparison with traditional estimators such as the periodogram highlight several strong points of the method. We also identify certain limitations, namely the instability of estimates for high noise levels. These limitations can be alleviated if *a priori* information about the signal is available. Two such problems are discussed in which the information at hand has the form of a constraint on the input signal-to-noise ratio.

We show how such information can be incorporated in the maximum-likelihood estimation procedure. First we assume the signal power to be known. Theoretical issues of existence and uniqueness of the solution are discussed. We proceed with a problem in which the information is less complete, when only an upper-bound on the signal power is available. The statistical performance of both constrained estimators is quantitatively studied.

January 17, 1989

* This work was supported by contract number N00014-86-K-0370 from the Office of Naval Research.

Maximum-Likelihood Spectrum Estimation of Periodic Processes from Noisy Data *

P. Moulin
D. L. Snyder
J. A. O'Sullivan

Electronic Systems and Signals Research Laboratory
Department of Electrical Engineering
Washington University
Saint Louis, MO 631[illegible]0

1. Introduction

A promising approach to maximum-likelihood estimation of Toeplitz constrained covariance matrices has been proposed recently [1]. Several further developments can be considered. First, this method also applies to the dual problem of spectrum estimation. Another issue of interest is that the statistical model can account for the presence of additive noise corrupting the observations and for linear transformations of the process whose covariance or spectrum is sought. These considerations have motivated a new approach to high-resolution delay-doppler radar imaging, where a major goal is to produce estimates of the target's scattering function [2]. In the special case of a point target and a constant envelope transmitted signal, this reduces to a spectrum estimation problem.

This paper describes some recent developments for this problem. We study the statistical performance of the new maximum-likelihood spectrum estimator both theoretically and numerically. Comparison with traditional estimators such as the periodogram highlight several strong points of the method. We also identify certain limitations, namely the instability of estimates for high noise levels. These limitations can be alleviated if *a priori* information about the signal is available. Two such problems are discussed here in which the information at hand has the form of a constraint on the input signal-to-noise ratio.

This paper is organized as follows. Our model is presented in Section 2. A maximum-likelihood formulation of the problem is given in Section 3, and the equations are solved via the expectation-maximization algorithm. Section 4 is devoted to a statistical performance analysis of this estimator and a comparison with two other methods. In Section 5 we show how *a priori* information on the signal can be incorporated in the maximum-likelihood estimation procedure. First we assume the signal power to be known. Theoretical issues of existence and uniqueness of the solution are discussed. Section 5 deals with a less complete knowledge, where only an upper-bound on the signal power is available. The last section is devoted to a quantitative study of the statistical performance of both constrained estimators.

2. Model

The following is derived from the model presented in [1] for a point target and a constant envelope transmitted signal. The observation is an N-vector sample of a wide-sense stationary, periodic, Gaussian process corrupted by an additive noise :

$$r = b + w \,, \tag{2.1}$$

where b contains N consecutive samples of a zero-mean periodic process b_p with length $P \geq N$, and w is an zero-mean white Gaussian noise with variance N_0, uncorrelated with b.

* This work was supported by contract number N00014-86-K-0370 from the Office of Naval Research.

The periodicity assumption is required to guarantee that the likelihood function is bounded above; therefore, there exists a maximum-likelihood estimator [1].

Now we define the spectral process associated with b_p to be the DFT of one period of b_p. Assume that we are interested in estimating only M of the components of this spectral P-vector ($1 \leq M \leq P$), the other components being zero with probability 1 ; let c be this M-vector. This assumption is introduced to deal with the bandlimited spectra encountered in radar applications, which arise because radar targets have finite extent [2]. c is a Gaussian random M-vector with diagonal covariance Σ, whose entries $\sigma^2(i)$, i = 0,..,M-1, are real and positive. c and b are related by a linear transformation :

$$b = \Gamma^\dagger c \ , \tag{2.2}$$

where we have defined the $M \times N$ matrix Γ, consisting of the first N rows and the outer M columns of the $P \times P$ DFT matrix. The superscript $\dagger$ denotes the Hermitian-transpose operator on matrices.

Our model for the observations can now be written as

$$r = \Gamma^\dagger c + w \ . \tag{2.3}$$

The covariance matrix for r is given by

$$K_r = E[rr^\dagger] = \Gamma^\dagger \Sigma \Gamma + N_0 I_N \ , \tag{2.4}$$

where I_N is the $N \times N$ identity matrix.

3. Spectrum Estimators

In this section we introduce a maximum-likelihood spectrum estimator for the model (2.3), denoted by ML1. We also define two estimators which will be analyzed and compared to ours in the next section. The first one is the maximum-likelihood estimator derived assuming noise-free data, denoted by ML0 ; the second one is the periodogram.

3.1. ML1 Estimator

From (2.4), the likelihood function for Σ is

$$L(r,\Sigma) = -\tfrac{1}{2} \ln \det (\Gamma^\dagger \Sigma \Gamma + N_0 I_N) - \tfrac{1}{2}\, r^\dagger (\Gamma^\dagger \Sigma \Gamma + N_0 I_N)^{-1} r \ . \tag{3.1}$$

Maximizing the likelihood with respect to Σ yields the necessary trace condition which the estimate $\hat{\Sigma}$ must satisfy [1,2]:

$$Tr\, [\Gamma (\Gamma^\dagger \hat{\Sigma} \Gamma + N_0 I_N)^{-1} (rr^\dagger - \Gamma^\dagger \hat{\Sigma} \Gamma - N_0 I_N)(\Gamma^\dagger \hat{\Sigma} \Gamma + N_0 I_N)^{-1} \Gamma^\dagger \delta\hat{\Sigma}] = 0 \ , \tag{3.2}$$

for all $M \times M$ diagonal matrices $\delta\hat{\Sigma}$. This trace condition is a nonlinear equation in $\hat{\Sigma}$. Generally it cannot be solved directly in closed-form, so some numerical search procedure must be implemented. An elegant solution is the expectation-maximization (EM) algorithm used in [1,2]. An initial estimate $\hat{\Sigma}^{(0)}$ is selected. At step k+1 (k = 0,1,..) the estimate is updated according to

$$\hat{\Sigma}^{(k+1)} = argmax\ Q(\Sigma | \hat{\Sigma}^{(k)}) \tag{3.3}$$

where

$$Q(\Sigma | \hat{\Sigma}^{(k)}) = -\tfrac{1}{2} \sum_{i=0}^{M-1} \ln \sigma^2(i) - \tfrac{1}{2} \sum_{i=0}^{M-1} \frac{E[\,|c(i)|^2 \,|\, r, \hat{\Sigma}^{(k)}]}{\sigma^2(i)} \ , \tag{3.4}$$

and

$$E[\,|c(i)|^2 \,|\, r, \hat{\Sigma}^{(k)}] = [\hat{\Sigma}^{(k)} - \hat{\Sigma}^{(k)} \Gamma (\Gamma^\dagger \hat{\Sigma}^{(k)} \Gamma + N_0 I_N)^{-1} \Gamma^\dagger \hat{\Sigma}^{(k)} + \hat{\Sigma}^{(k)} \Gamma (\Gamma^\dagger \hat{\Sigma}^{(k)} \Gamma + N_0 I_N)^{-1}$$
$$\times rr^\dagger (\Gamma^\dagger \hat{\Sigma}^{(k)} \Gamma + N_0 I_N)^{-1} \Gamma^\dagger \hat{\Sigma}^{(k)}]\,(i,i) \ . \tag{3.5}$$

This algorithm produces a sequence of estimates

$$\hat{\sigma}^2(i)^{(k+1)} = E[\,|c(i)|^2 \,|_r, \hat{\Sigma}^{(k)}] \tag{3.6}$$

having increasing likelihood. It can be shown that the stable points of this algorithm satisfy the necessary trace condition for a maximizer [2]. The issue of uniqueness is addressed in [3].

Special case : $N = M = P = 1$

A closed-form expression for $\hat{\Sigma}$ can be derived in this special case:

$$\hat{\sigma}^2(i) = \max(0, r^2 - N_0) \, . \tag{3.7}$$

3.2. ML0 Estimator

Additive noise corrupting observations is usually not included separately in approaches to spectrum estimation. This model was assumed in [1]. The sequence of estimates of Σ is still given by (3.6) and (3.5), in which we now let $N_0 = 0$. We call this the ML0 estimation. Clearly ML0 and ML1 are equivalent for noise-free problems.

Special case : $N = M$

The problem for which the number of observations (N) is equal to the number of parameters to be estimated (M) is of some practical interest. It also turns out that the trace condition can be solved in closed-form in this instance. The matrix Γ is then invertible, indicating the existence of a one-to-one mapping between r and c. The ML0 estimator is simply

$$\hat{\sigma}^2(i) = |(\Gamma^{-\dagger} r)(i)|^2 \, , \tag{3.8}$$

where $\Gamma^{-\dagger}$ denotes $(\Gamma^{-1})^{\dagger}$.

3.3. Periodogram

The periodogram estimate of the spectrum is defined as the (scaled) magnitude-squared Fourier transform of the N observations padded with P-N zeroes [4]. The first M spectrum samples are then given by

$$\hat{\sigma}^2(i) = (P/N) \, |(\Gamma r)(i)|^2 \tag{3.9}$$

Special case : $N = M = P$

When N = M = P, the matrix Γ is equal to the $P \times P$ DFT matrix and the periodogram and ML0 estimates are the same. In this case, a full period of the process is estimated.

4. Performance Analysis

In this section, we estimate Σ for the model (2.3) and study the statistical performance of the three estimators above. For each method the bias and variance are evaluated, where

$$Bias[\hat{\Sigma}] = E[\hat{\Sigma}] - \Sigma \tag{4.1}$$

and

$$Var[\hat{\Sigma}] = E[\hat{\Sigma}^2] - (E[\hat{\Sigma}])^2 \, . \tag{4.2}$$

As we shall see in Section 4.3, the performance strongly depends upon the input signal to noise ratio defined by

$$SNR_{in} = E_0 \, / \, N_0 \, , \tag{4.3}$$

where E_0 is the average power of the process, defined by

$$E_0 = (1/P) \, Tr \, [\Sigma] \, . \tag{4.4}$$

From (4.1) and (4.2), we derive the mean-squared error (MSE) matrix, defined by

$$MSE \, [\hat{\Sigma}] = E[(\hat{\Sigma} - \Sigma)^2] = Var[\hat{\Sigma}] + (Bias[\hat{\Sigma}])^2 \, . \tag{4.5}$$

The output signal to noise ratio matrix is defined as follows :

$$SNR_{out}[\hat{\Sigma}] = E[\hat{\Sigma}] \, (MSE \, [\hat{\Sigma}])^{-\frac{1}{2}} \, . \tag{4.6}$$

In the following section, we evaluate the bias and mean-squared error for the estimators derived in Section 3. Whenever closed-form expressions for the ML estimates cannot be derived, computer simulations are performed. Typically 3000 realizations are generated for each process. For a given estimator, (4.1) and (4.6) are then estimated from the 3000 estimates.

4.1. Performance Analysis

Closed form expressions for the bias and mean-squared error are derived for ML0 and the periodogram when possible. Simulations were carried out to compare the performance of the estimators for various levels of input SNR. The performance was then compared to the Cramer-Rao lower bound for the variance of unbiased estimators. Much effort was made for the special case M = N. This provides insight into the problem since the ML0 equations can be solved in closed form. The choice of P is free, so long as $P \geq N$ [2].

4.2. Closed-form Expressions for Estimator Performance

(a) ML1

As indicated in Section 3.1, no closed-form expression for the estimator is available, so the evaluation of bias and variance is obtained by computer simulation.

(b) ML0

Closed-form expressions for ML0 can be derived when M = N. The results are presented below.

Bias

Combining (2.3) and (3.8), we can write

$$\hat{\sigma}^2(i) = |(c + \Gamma^{-\dagger} w)(i)|^2 \, . \tag{4.7}$$

Taking the expectation of (4.7), we get

$$E[\hat{\sigma}^2(i)] = \sigma^2(i) + N_0 (\Gamma\Gamma^\dagger)^{-1}(i,i) \, , \tag{4.8}$$

which implies

$$Bias[\hat{\sigma}^2(i)] = N_0 (\Gamma\Gamma^\dagger)^{-1}(i,i) \, . \tag{4.9}$$

The bias is due to the noise corrupting the observations and is proportional to its variance. The sensitivity of the bias to the noise is determined by the diagonal entries of the matrix $(\Gamma\Gamma^\dagger)^{-1}$.

Mean-Squared Error

Taking the expectation of (4.7) squared, we obtain

$$E[(\hat{\sigma}^2(i))^2] = \sigma^4(i)\,(2+\delta_{i0}) + N_0\,\sigma^2(i)\,\Big(\,4(\Gamma\Gamma^\dagger)^{-1}(i,i) + 2\sum_{j=0}^{M-1} \mathrm{Re}[\Gamma^{-\dagger}(i,j)^2]\,\Big)$$

$$+ N_0^2\,\Big(\,2(\Gamma\Gamma^\dagger)^{-1}(i,i)^2 + |\sum_{j=0}^{M-1} \Gamma^{-\dagger}(i,j)^2|^2\,\Big) \, . \tag{4.10a}$$

After some algebraic manipulations, this expression can be lower-bounded by

$$E[(\hat{\sigma}^2(i))^2] \geq 2\,[\sigma^2(i) + N_0(\Gamma\Gamma^\dagger)^{-1}(i,i)]^2 = 2\,(\,E[\hat{\sigma}^2(i)]\,)^2 \, . \tag{4.10b}$$

From (4.8) and (4.10), (4.5) becomes

$$MSE\,[\hat{\sigma}^2(i)] = (\,E[(\hat{\sigma}^2(i))]\,)^2 + (N_0\,(\Gamma\Gamma^\dagger)^{-1}(i,i)\,)^2 \, , \tag{4.11a}$$

and

$$MSE\,[\hat{\sigma}^2(i)] \geq \sigma^4(i) + 2\,\sigma^2(i)\,N_0\,(\Gamma\Gamma^\dagger)^{-1}(i,i) + 2\,(N_0\,(\Gamma\Gamma^\dagger)^{-1}(i,i))^2 \, . \tag{4.11b}$$

(c) Periodogram

Bias

Combining (2.3) and (3.9), we write the periodogram estimates in the equivalent form

$$\hat{\sigma}^2(i) = (P/N)\,|\,(\Gamma\Gamma^\dagger c + \Gamma w)(i)|^2\ . \tag{4.12}$$

Taking the expectation of (4.12), we get

$$E[\hat{\sigma}^2(i)] = (P/N)\,(\Gamma\Gamma^\dagger\Sigma\Gamma\Gamma^\dagger + N_0\Gamma\Gamma^\dagger)(i,i)\ , \tag{4.13}$$

and

$$Bias[\hat{\sigma}^2(i)] = (\ (P/N)\,(\Gamma\Gamma^\dagger\Sigma\Gamma\Gamma^\dagger) - \Sigma\ )(i,i) + (P/N)\,N_0\,(\Gamma\Gamma^\dagger)(i,i)\ . \tag{4.14}$$

The bias contains two terms. The second is due to the noise and is proportional to N_0. The sensitivity of the bias to the noise is determined by the diagonal entries of the matrix $\Gamma\Gamma^\dagger$. The other term is independent of N_0. Even for noise-free observations, the periodogram is a biased estimator of Σ unless $\Gamma\Gamma^\dagger$ is the identity matrix. This would be the case only for N = M = P (observation of a full period of the process) or N/M $\rightarrow \infty$ (infinite data).

Mean-Squared Error

Taking the expectation of (4.12) squared, we obtain

$$\begin{aligned} E[(\hat{\sigma}^2(i))^2] = (P^2/N^2)\ [\ 2\ [\sum_{j=0}^{M-1}\sigma^2(j)\,|\,(\Gamma\Gamma^\dagger)(i,j)|^2]^2 + 4\,N_0\sum_{j=0}^{M-1}\sigma^2(j)\,|\,(\Gamma\Gamma^\dagger)(i,j)|^2\,(\Gamma\Gamma^\dagger)(i,i) \\ + 2N_0^2\,(\Gamma\Gamma^\dagger)(i,i)^2 \\ +\ |\ \sigma^2(0)\,(\Gamma\Gamma^\dagger)(i,0)^2 + \sigma^2(M/2)\,(\Gamma\Gamma^\dagger)(i,M/2)^2 + N_0\sum_{j=0}^{M-1}\Gamma(i,j)^2\,|^2\ ]\ . \end{aligned} \tag{4.15a}$$

This expression is lower-bounded by

$$2\,(P/N)^2\ [\ (\Gamma\Gamma^\dagger\Sigma\Gamma\Gamma^\dagger + N_0\Gamma\Gamma^\dagger)(i,i)\ ]^2 = 2\ (\ E[\hat{\sigma}^2(i)]\ )^2\ . \tag{4.15b}$$

From (4.13) and (4.15), (4.5) becomes

$$MSE\ [\hat{\sigma}^2(i)] = (\ E[\hat{\sigma}^2(i)]\ )^2 + [\ (P/N)\,(\Gamma\Gamma^\dagger\Sigma\Gamma\Gamma^\dagger - (N/P)\,\Sigma + N_0\Gamma\Gamma^\dagger)(i,i)\ ]^2\ , \tag{4.16a}$$

and

$$\begin{aligned} MSE\ [\hat{\sigma}^2(i)] \geq (P^2/N^2)\ (\ [(\Gamma\Gamma^\dagger\Sigma\Gamma\Gamma^\dagger)(i,i)^2 + (\Gamma\Gamma^\dagger\Sigma\Gamma\Gamma^\dagger - (N/P)\,\Sigma)(i,i)^2] \\ + 2\,N_0\,(\Gamma\Gamma^\dagger)(i,i)\,(2\,\Gamma\Gamma^\dagger\Sigma\Gamma\Gamma^\dagger - (N/P)\,\Sigma)(i,i) \\ + 2\ [\ N_0\,(\Gamma\Gamma^\dagger)(i,i)]^2\ )\ . \end{aligned} \tag{4.16b}$$

4.3. Simulation results

Process 1

The first process we consider is real and has period P = 10. Its spectrum is symmetric and lowpass (M = 5). All nonzero spectrum samples are identical :

$$\sigma^2(i) = 1\ , \qquad i = 0,..,4\ .$$

The number of observations is N = M = 5.

The noise variance N_0 ranges from 0 to 1. Figures 1 and 2 show the bias and SNR_{out} for the estimators of $\sigma^2(2)$ as a function of SNR_{in}, according to the definitions (4.1), (4.3), and (4.6). In the absence of additive noise ($SNR_{in} \rightarrow \infty$), ML1 and ML0 are the same. Both are unbiased estimators. The periodogram, however, is biased, and its MSE is also larger than the MSE for the ML estimators. When N_0 increases from 0, the performance of the estimators is roughly constant so long as SNR_{in} remains above some threshold. For larger N_0, all three estimators exhibit a strong degradation in

performance. Comparing the thresholds for ML0 and ML1, we see the tremendous improvements brought by taking the noise into account in the model. Typically, for a same SNR_{out}, ML1 will have the same performance as ML0 operating in a 20 dB noisier environment.

We also notice that the threshold for the periodogram is located at a lower SNR_{in} than for the ML estimators. In Sections 4.2(b) and 4.2(c), we indicated how the sensitivity of the performance to noise can be determined for ML0 and the periodogram when N = M. It turns out that for the flat-spectrum process considered here, the periodogram has a lower sensitivity than ML0 and ML1. This is thought to be due to the smooth spectrum used in the simulation.

Process 2

It has been conjectured that the periodogram does not perform well for nonuniform spectra [5]. This motivated our study of a sharply peaked spectrum. The process has period P = 10, and a single nonzero spectrum component

$$\sigma^2(0) = 1 .$$

There is just N = M = 1 observation.

Bias and SNR_{out} for the estimators of $\sigma^2(0)$ are plotted as a function of SNR_{in} in Figures 3 and 4. In the absence of additive noise, the periodogram is very strongly biased, and its MSE is large. Furthermore, in high-noise environment the periodogram is no longer more robust than the ML estimators. Clearly, the periodogram is outperformed by ML0 and ML1. It should also be noticed that for this process, the improvement of ML1 over ML0 is quite reduced.

Computational Considerations

The convergence rate of the EM algorithm depends on several parameters. The computation time for each iteration is of order $M N^2$. The number of iterations required for convergence of the algorithm grows as M and N increase. For ML1, more iterations are required as N_0 increases, especially in the threshold region and beyond. Typical figures are: for process 1 with $N_0 = 0.1$, 30 iterations are required before the spectrum estimates are stable; when $N_0 = 1$, 300 iterations must be performed. Our algorithm is implemented on a Masscomp model 5500. Running the program on 3000 realizations in the latter case is typically completed in 6 CPU hours. We are presently implementing these algorithms on a mesh-connected 1024 processor (DAP by Active Memory Technology), and we expect a major reduction in the time required to produce estimates.

4.4. Cramer-Rao Bounds

In this section, we study how the MSE of the estimators considered so far relates to the Cramer-Rao bound on the variance. The Cramer-Rao bound on the variance of any unbiased (UB) estimator of $\hat{\sigma}^2(i)$ for our model has been found to be [3]

$$UB\text{–}CR[\hat{\sigma}^2(i)] = (\sigma^2(i) + N_0(\Gamma\Gamma^\dagger)^{-1}(i,i))^2 . \tag{4.17}$$

From (4.5) and (4.17), the MSE for an unbiased estimator whose variance attains the Cramer-Rao bound is given by

$$MSE[\hat{\sigma}^2(i)] = (\sigma^2(i) + N_0(\Gamma\Gamma^\dagger)^{-1}(i,i))^2 . \tag{4.18}$$

Next we state the Cramer-Rao bound on the variance of a biased (B) estimator of $\hat{\sigma}^2(i)$:

$$B\text{–}CR[\hat{\sigma}^2(i)] = UB\text{–}CR[\hat{\sigma}^2(i)] \left(\frac{\partial E[\hat{\sigma}^2(i)]}{\partial \sigma^2(i)}\right)^2 . \tag{4.19}$$

From (4.5), (4.17) and (4.19), the MSE for a biased estimator reaching the Cramer-Rao bound is given by

$$MSE[\hat{\sigma}^2(i)] = (\sigma^2(i) + N_0(\Gamma\Gamma^\dagger)^{-1}(i,i))^2 \left(\frac{\partial E[\hat{\sigma}^2(i)]}{\partial \sigma^2(i)}\right)^2 + (Bias[\hat{\sigma}^2(i)])^2 . \tag{4.20}$$

From the analytical expressions given for $E[\hat{\sigma}^2(i)]$ in Section 4.2, we can now calculate the gradient of $E[\hat{\sigma}^2(i)]$ for ML0 and the periodogram. Then, the minimum MSE for a biased estimator having the

same bias as ML0 and the periodogram is derived, and a comparison with the actual MSE is made. No closed-form expression has been found for ML1.

ML0

From (4.7),

$$\frac{\partial E[\hat{\sigma}^2(i)]}{\partial \sigma^2(i)} = 1 \,. \tag{4.21}$$

From (4.9), (4.20) and (4.21), the MSE is lower-bounded by

$$MSE_{cr}[\hat{\sigma}^2(i)] = \sigma^4(i) + 2\,\sigma^2(i)\,N_0\,(\Gamma\Gamma^\dagger)^{-1}(i,i) + 2\,[\,N_0\,(\Gamma\Gamma^\dagger)^{-1}(i,i)\,]^2 \,. \tag{4.22}$$

Periodogram

From (4.13),

$$\frac{\partial E[\hat{\sigma}^2(i)]}{\partial \sigma^2(i)} = (P/N)\,(\Gamma\Gamma^\dagger\Gamma\Gamma^\dagger)(i,i) \,. \tag{4.23}$$

Combining (4.14), (4.20) and (4.23), the MSE is lower-bounded by

$$\begin{aligned} MSE_{cr}\,[\hat{\sigma}^2(i)] = (P^2/N^2)\,(\,&[(\Gamma\Gamma^\dagger\Sigma\Gamma\Gamma^\dagger)(i,i)^2 + (\Gamma\Gamma^\dagger\Sigma\Gamma\Gamma^\dagger - (N/P)\,\Sigma)(i,i)^2] \\ &+ 2\,N_0\,(\Gamma\Gamma^\dagger)(i,i)\,(2\,\Gamma\Gamma^\dagger\Sigma\Gamma\Gamma^\dagger - (N/P)\,\Sigma)(i,i) \\ &+ 2\,[\,N_0\,(\Gamma\Gamma^\dagger)(i,i)]^2\,) \,. \end{aligned} \tag{4.24}$$

Comparison of MSE's with Cramer-Rao bounds

The Cramer-Rao bounds (4.22) and (4.24) on the MSE are the same as the bounds (4.11b) and (4.16b) derived algebraically from the exact expressions (4.11a) and (4.16a). Figure 5 shows how the lower bounds compare with the exact expressions for Process 1. The actual MSE's are 3-4 dB above their respective bounds.

4.5. Discussion

The results derived above suggest additional comments on a comparison between periodogram and ML estimators. Typically each component of the gradient of $E[\hat{\sigma}^2(i)]$ given in (4.23) is much smaller than unity (for the processes we consider), and the Cramer-Rao bound on the variance of the periodogram-like biased estimator is much smaller than the Cramer-Rao bound on the variance of unbiased estimators. When the variance dominates the MSE, the periodogram offers a good MSE performance. This was the case for Process 1. For a less uniform spectrum such as the one chosen for Process 2, the bias dominates the MSE and the periodogram is outperformed by the ML estimators.

5. Constrained maximum-likelihood estimation

5.1. Description of the problem

An examination of Figures 1-4 suggests that ML1 suffers in certain situations. When SNR_{in} is low, the estimates are biased and their variance is large. Although the maximum-likelihood estimator is asymptotically unbiased and efficient, these properties are not guaranteed in the small-sample problems considered in Section 4. This limitation can be alleviated if *a priori* knowledge, such as SNR_{in}, is available. Since N_0 is known, such a constraint on the signal-to-noise ratio can be translated into a constraint on the signal power that must be satisfied by the maximum-likelihood estimates. Now we show how this constraint can be incorporated into the EM algorithm. The constrained estimates exist and are unique.

In Section 5.2, SNR_{in} is known. In Section 5.3, our knowledge is more incomplete, and only an upper bound on SNR_{in} is available.

5.2. Known SNR_{in}

The equations for ML1 presented in Section 3.1 can be modified as follows to satisfy the constraint. At each step of the EM algorithm, we maximize $Q(\Sigma \mid \hat{\Sigma}^{(k)})$ defined in (3.4), subject to the power constraint

$$\sum_{i=0}^{M-1} \sigma^2(i) = PE_0 = S \,, \tag{5.1}$$

where E_0 is the signal power. The solution also maximizes

$$Q(\Sigma \mid \hat{\Sigma}^{(k)}) + \lambda \left(\sum_{i=0}^{M-1} \sigma^2(i) - S \right), \tag{5.2}$$

where λ is a Lagrange multiplier. Taking the gradient of (5.2) with respect to Σ, we obtain a quadratic equation for each spectral component

$$2\,\lambda\,\sigma^4(i) - \sigma^2(i) + C_i = 0 \,, \tag{5.3}$$

where

$$C_i = E[\,|c(i)|^2 \,|r, \hat{\Sigma}^{(k)}]$$

is calculated according to (3.5). The solution to (5.3) is

$$\begin{aligned} \sigma^2(i) &= \frac{1 + I_i\sqrt{1-8C_i\lambda}}{4\lambda} \quad &: \lambda \neq 0 \\ &= C_i &: \lambda = 0 \,, \end{aligned} \tag{5.4}$$

where I_i is either +1 or -1. The equation for λ is

$$4S\lambda - M = \sum_{i=0}^{M-1} I_i\sqrt{1-8C_i\lambda} \,. \tag{5.5}$$

In general this nonlinear equation in λ cannot be solved in closed-form. Furthermore, an ambiguity subsists about the choice of the signs I_i. The latter problem is solved by application of the following theorem :

Theorem

Assume that $C_0 > C_i$, i = 1,..,M-1. Then

(1)

$$\begin{aligned} I_i &= -1 \quad : i = 1,..,M-1 \\ I_0 &= +1 \quad : S < 2C_0\,[M - \sum_{i=1}^{M-1} I_i\sqrt{1-(C_i/C_0)}\,] \\ &= -1 \quad : else \end{aligned}$$

(2) λ is the largest nonzero solution of

$$(\,4S\lambda - M + \sum_{i=1}^{M-1} I_i\sqrt{1-(C_i/C_0)}\,)^2 = 1 - 8C_0\lambda, \quad \text{for} \quad S \neq \sum_{i=1}^{M-1} C_i \,, \tag{5.6a}$$

and

$$\lambda = 0, \quad \text{for} \quad S = \sum_{i=1}^{M-1} C_i. \tag{5.6b}$$

λ is upper-bounded by $1/8C_0$, and (5.6a) can be solved numerically for λ. Note that the particular case (5.6b) is also the solution to the unconstrained maximization problem. Next, $\hat{\sigma}^2(i)^{(k+1)}$ is calculated from (5.4). The whole procedure is repeated at each maximization step of the EM algorithm. Note that because of the highly nonlinear nature of the problem, no analytic expression is available for the constrained estimator, even in the special case mentioned in (3.7).

5.3. Known upper bound on SNR_{in}

In this section, the *a priori* knowledge about SNR_{in} has the form of an upper bound. Our approach parallels that of the previous section, with the upper bound now expressed as an inequality constraint on the estimated signal power. At each step of the EM algorithm, we maximize $Q(\Sigma \mid \hat{\Sigma}^{(k)})$ defined in (3.4), subject to the inequality constraint

$$\sum_{i=0}^{M-1} \sigma^2(i) \leq PE_0 = S \,, \tag{5.7}$$

where E_0 is the upper bound on the signal power. If the unconstrained solution satisfies the upper bound, the constraint is inactive and the estimate is given by (3.6). Otherwise, the constraint is active, and as in Section 5.2, the solution is the maximizer of the expression (5.2).

We can expect the performance of this estimator to be strongly conditioned by the choice of E_0. In the limiting case $E_0 \rightarrow \infty$, the constraint is always inactive and the estimator is equivalent to the unconstrained estimator. For the other extreme case $E_0 \rightarrow 0$, the constraint is always active.

6. Simulation results

In this section, we apply the SNR-constrained estimators derived above to Process 1, and we evaluate numerically both their bias and mean-squared error.

Figures 6 and 7 give a plot of the bias and SNR_{out} for different estimators of $\sigma^2(2)$ as a function of SNR_{in}, according to the definitions (4.1), (4.3), and (4.6). The estimators represented on these figures are: the two constrained estimators of Section 5, respectively denoted by EQ-MLE and INEQ-MLE, and defined for the (true) power constraint $S = 5$; the unconstrained estimator ML1 of Section 3.1; and the periodogram PER of Section 3.3.

In the absence of additive noise ($SNR_{in} \rightarrow \infty$), ML1 and EQ-MLE are unbiased. The periodogram and INEQ-MLE, however, are biased. For the latter, this can be understood as follows. The sum of the M estimates is smaller or equal to $S = 5$, and therefore the sum of all biases is negative. When N_0 increases from 0, the performance of the estimators is roughly constant so long as SNR_{in} remains above some threshold. For larger N_0, all estimators exhibit a degradation in performance. Note that for the SNR-constrained estimators, each bias is upper-bounded by $S - \sigma^2(i)$, and lower-bounded by $-\sigma^2(i)$. Comparing the SNR_{out} performance in Figure 2, we see the favorable effects of incorporating SNR constraints into the problem. For low N_0, SNR_{out} is improved. This is due to the estimates having a lower variance, which is the dominant term in SNR_{out}. For very noisy data, the performance of the estimators is clearly improved. We can easily derive a lower bound for $SNR_{out}[\hat{\sigma}^2(i)]$:

$$\frac{\sigma^2(i)}{\max\left[S - \sigma^2(i)\,,\, \sigma^2(i)\right]} \leq 1 \,.$$

This bound is independent of N_0.

Conclusions

In this paper, we have described an approach to spectrum estimation from noisy data, based upon a statistical model for the observations. First we derive a maximum-likelihood estimator, and evaluate its statistical performance. A comparison is made with two other methods that do not take the additive noise into account. One is the traditional periodogram and the other is the maximum-likelihood estimator derived for a noise-free model. It is shown that in terms of bias and MSE, the new estimator can offer a better performance than the latter ones. The improvement over the periodogram is noticeable for rough spectra: The MSE was 15 dB lower for the process we considered.

In general however, the maximum-likelihood estimates are still unstable at high noise levels. In the second step of our study, we refine our technique to improve the performance when some side information exists. We have studied one such problem in which some information about the signal-to-noise ratio is available. The performance for the SNR-constrained estimators has been numerically evaluated, and compared with that of the unconstrained estimator and of the periodogram. The new estimators perform significantly better than their competitors for low SNR_{in}. Because of the SNR

constraint, the estimates are not allowed to take on the large values that were produced in the unconstrained estimation problem. This results in the estimates having a lower variance. One additional feature of our approach, and an attractive one, is its versatility. Only a slight modification of the (unconstrained) algorithm is required.

References

[1] M. I. Miller, D. L. Snyder, "The Role of Likelihood and Entropy in Incomplete-Data Problems: Applications to Estimating Point-Process Intensities and Toeplitz Constrained Covariances," *Proc. IEEE, Vol.75,* No.7, July 1987.

[2] D. L. Snyder, J. A. O'Sullivan, M. I. Miller, "The Use Of Maximum-Likelihood Estimation For Forming Images Of Diffuse Radar-Targets From Delay-Doppler Data," *IEEE Trans. on Information Theory,* to appear in 1989.

[3] J. A. O'Sullivan, P. Moulin, D. L. Snyder, "Cramer-Rao Bounds for Constrained Spectrum Estimation with Application to a Problem in Radar Imaging", *Proc. of the 1988 Allerton Conference.*

[4] W. Davenport, W. Root, *Random Signals and Noise,* McGraw Hill, 1958.

[5] D. Fuhrmann, personal communication.

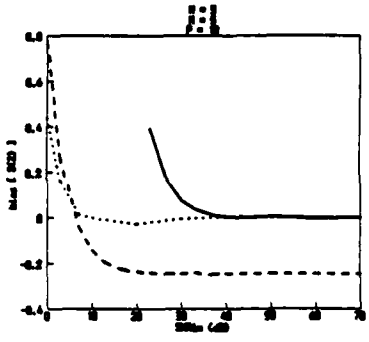

Figure 1. $Bias(\sigma^2(2))$ for Process 1

ML0 (solid line), ML1 (dotted line), periodogram (dashed line)

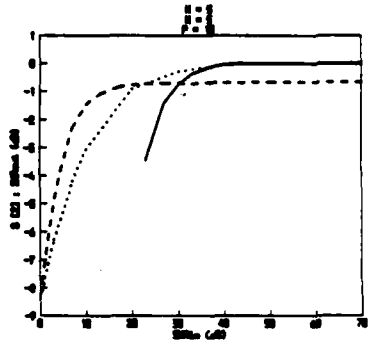

Figure 2. $SNR_{out}(\sigma^2(2))$ for Process 1

ML0 (solid line), ML1 (dotted line), periodogram (dashed line)

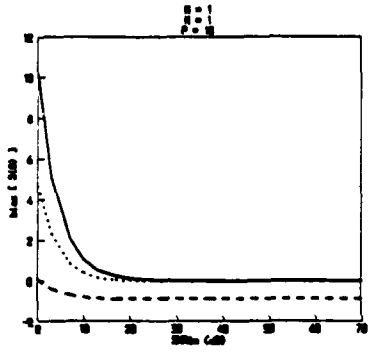

Figure 3. $Bias(\sigma^2(0))$ for Process 2

ML0 (solid line), ML1 (dotted line), periodogram (dashed line)

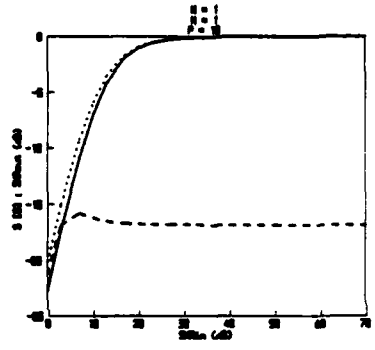

Figure 4. $SNR_{out}(\sigma^2(0))$ for Process 2

ML0 (solid line), ML1 (dotted line), periodogram (dashed line)

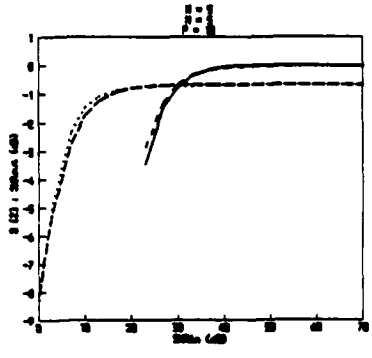

Figure 5. Comparison of $SNR_{out}(\sigma^2(2))$ and Cramer-Rao bounds for Process 1

ML0 (solid line), its CR bound (short-dashed line), periodogram (long-dashed line), its CR bound (dotted line)

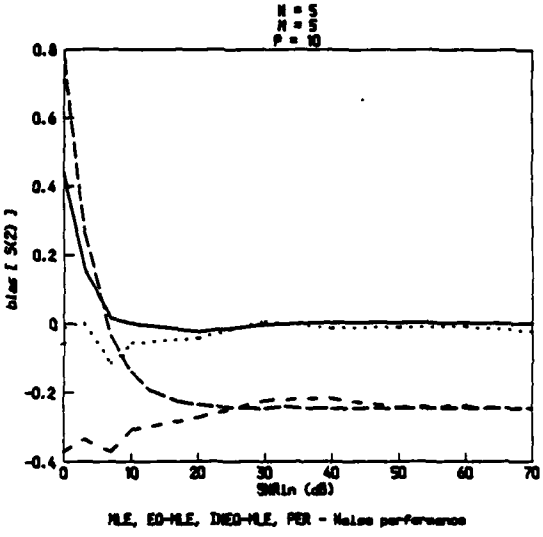

Figure 6. $Bias(\sigma^2(2))$
ML1 (solid line), EQ-MLE (dotted line), INEQ-MLE (short-dashed line), periodogram (long-dashed line)

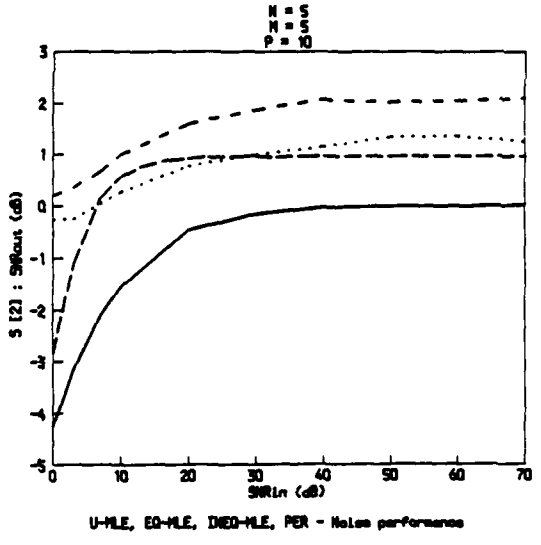

Figure 7. * $SNR_{out}(\sigma^2(2))$
ML1 (solid line), EQ-MLE (dotted line), INEQ-MLE (short-dashed line), periodogram (long-dashed line)

* Currently we are redrawing Figure 7 in which a former definition of the output signal-to-noise ratio was adopted.

4.2. Appendix 2. Status Report on Specular Imaging (K. Krause)

K. E. Krause
January 8, 1989

STATUS REPORT:

MAXIMUM LIKELIHOOD APPROACH TO SPECULAR TARGET IMAGING

The following summarizes activity between June of 1988 and January of 1989 in the statistical model formulation and imaging approach for the Maximum Likelihood Estimation based imaging of delay and doppler spread specular targets.

At the time of the last report, two concepts were identified for further analysis and possible selection as the theoretical model to use in the specular target imaging problem. They were: (1) Maximization of a likelihood function which is assumed to factor into a product of identically structured likelihood functions, one for each scatterer in the delay-doppler plane and (2) Application of the EM algorithm to the likelihood function in quest of a complete/incomplete data space formulation which would cause the factorization as described in (1) above to occur.

The consequence of the factorizations mentioned is to reduce a multi-dimensional problem to the complexity of a one-dimensional problem that will be solved many times, once for each point in the target space grid. The idea in investigating the EM algorithm was to provide a rigorous justification for this likelihood factorization.

Recalling that each scatterer in the model under investigation is assumed to be characterized by a deterministic amplitude(to be estimated at each point in the target space to form the image) and a random phase(varying from known exactly to uniform - and to be integrated out in the estimation procedure), the EM algorithm was considered for a complete data space which consisted of a scatterer return plus white noise constituting the signal for each scatterer. By this construction, the signals for each scatterer were independent, hence the likelihood factorable in a theoretically rigorous manner from the start. The remaining issue was to work out the equations to see what, if any, computational complications might occur with this formulation. Limiting forms of the random phase were considered in some detail. Specifically, **phase known exactly** was first assumed and the equations for the Expectation and

Maximization steps worked out. The result was a one step iteration with equation form comparable to the solution that results in the non-EM approach. Added in the Scheme of computational complexity was the need to do a linear smoothing in the E step, which was easily done in this case. **Phase uniform** was considered next. The expectation to be evaluated took a very complex form, so it was decided to look at limiting cases to see how the formulation and computational complexity would proceed. In considering a high signal to noise ratio condition, the estimate could be theoretically calculated but would require doing a nonlinear smoothing to determine a constant required in the solution. The EM algorithm in this application then seems to provide the basis for a rigorously correct likelihood factorization resulting in a one step solution, but with increased calculational complexity.

In light of this complexity, and with the realization that any simulations and/or data that the model would be tested against would likely use stepped frequency waveforms(the complex envelope of which would make factorizations appear reasonable for the integration times that would be used), it was decided to proceed with a simulation to test the first, non-EM model formulation. Evaluation of results will determine the necessity to proceed with the EM approach. Currently, the first model concept is being coded for imaging of simulated data from simple generic targets. Its performance in comparison with standard imaging techniques will then be studied.

4.3. Appendix 3. U.S. Patent 4,768,156

United States Patent [19]

Whitehouse et al.

[11] **Patent Number: 4,768,156**

[45] **Date of Patent: Aug. 30, 1988**

[54] **IMAGING SYSTEM**

[75] Inventors: **Harper J. Whitehouse**, San Diego, Calif.; **Donald L. Snyder**, St. Louis, Mo.

[73] Assignee: **The United States of America as represented by the Secretary of the Navy**, Washington, D.C.

[21] Appl. No.: **861,490**

[22] Filed: **May 6, 1986**

[51] Int. Cl.[4] G06F 15/336; G06F 15/66

[52] U.S. Cl. 364/521; 342/179; 342/195; 382/42; 364/516

[58] Field of Search 364/516, 518, 521, 728; 382/42; 342/25, 26, 179, 189, 195, 196, 197

[56] **References Cited**

U.S. PATENT DOCUMENTS

4,244,029	1/1981	Hogan et al.	382/42
4,470,048	9/1984	Short, III	342/189
4,602,348	7/1986	Hart	382/42 X
4,673,941	6/1987	Van Der Mark	342/195 X

OTHER PUBLICATIONS

Okuyama et al.: High Speed Digital Image Processor With Special Purpose Hardware for Two-Dimensional Convolution. Rev. Sci. Instr., Oct. 1979, pp. 1208–1212.

Baier et al.: Two Dimensional Convolution Processor, IBM Technical Disclosure Bulletin, vol. 26, No. 9, Feb. 1984, pp. 4807–4808.

D. L. Snyder, "Algorithms and Architectures for Statistical Image Processing in Emission Tomography," in: Real Time Signal Processing VII, vol. 495, Society of Photo-Optical Instrumentation Engineers, pp. 109–111, 1984.

Prickett et al.: Principles of Inverse Synthetic Aperture Radar (ISAR) Imaging. IEEE Eascon Record, Sep. 1980, pp. 340–345.

J. Blaine et al., "Data Acquisition Aspects of Super–PETT," IEEE Trans. on Nuclear Science, vol. NS–29, pp. 544–547, Feb. 1982.

D. L. Snyder et al., "A Mathematical Model for Positron Emission Tomography Systems Having Time-of-Flight Measurements," IEEE Trans. on Nuclear Science, vol. NS–28, pp. 3575–3583, Jun. 81.

D. L. Snyder, "Some Noise Comparisons of Data–Collection Arrays for Emission Tomography–Systems Having Time–of–Flight Measurements," IEEE Trans. on Nuclear Science, vol. NS–29, No. 1, pp. 1029–1033, Feb. 1982.

D. L. Snyder and D. G. Politte, "Image Reconstruction From List–Mode Data in an Emission Tomography System Having Time of Flight Measurements," IEEE Trans. on Nuclear Science, vol. NS–20, No. 3, pp. 1843–1849, Jun. 1983.

M. Bernfeld, "CHIRP Doppler Radar," Proc. IEEE, vol. 72, No. 4, pp. 540–541, Apr. 1984.

D. L. Mensa et al., "Coherent Doppler Tomography For Microwave Imaging," Proc. IEEE, vol. 71, No. 2, pp. 254–261, Feb. 1983.

M. J. Prickett et al., "Stepped Frequency Radar Target Imaging," Private Correspondence.

Primary Examiner—Felix D. Gruber

Attorney, Agent, or Firm—Ervin F. Johnston; Thomas Glenn Keough

[57] **ABSTRACT**

An improved imaging system has applications to synthetic aperture radar, inverse synthetic aperture radar, delay-doppler radar, positron-emission topography sonar, radiometry and other applications having a target image provided by a series of data parameterized by a variable such as θ. A receiver structure includes a band-pass matched-filter, square law envelope-detector, specialized processing and convolving to produce the improved images irrespective that the radar signals have practical side lobe structures and other features. Despite the demands of specialized processing the architecture of the algorithm permits real-time implementations.

7 Claims, 1 Drawing Sheet

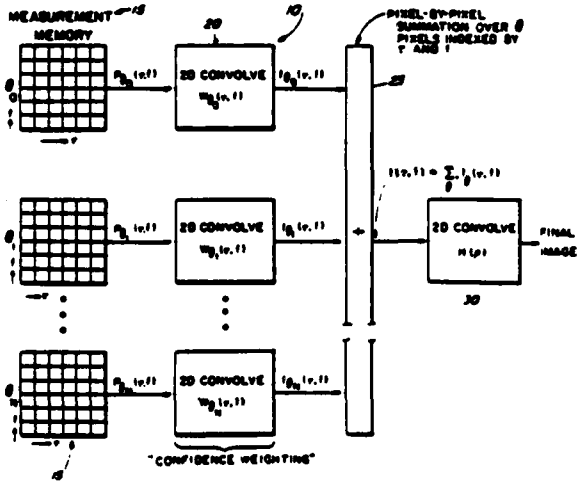

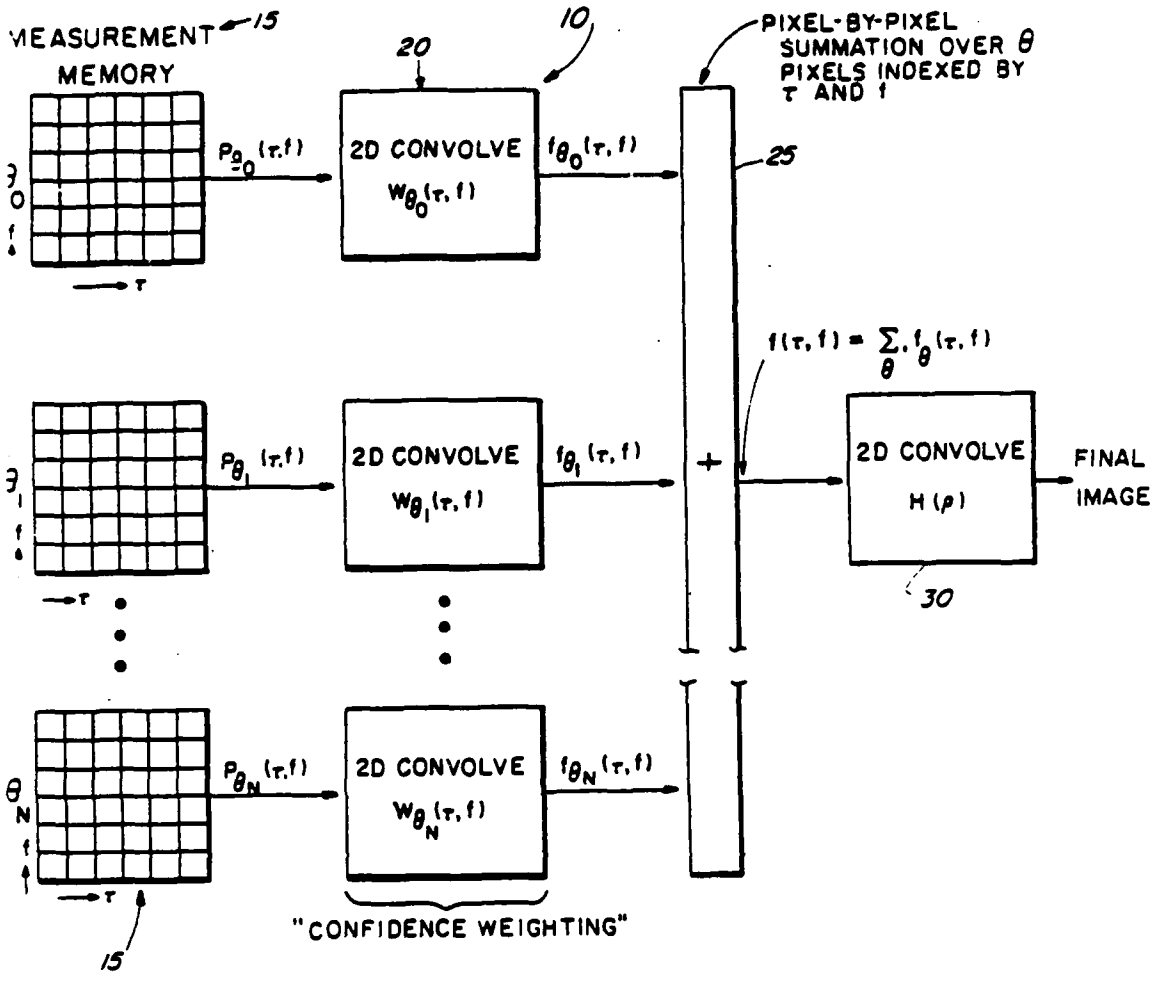

FIG. 1

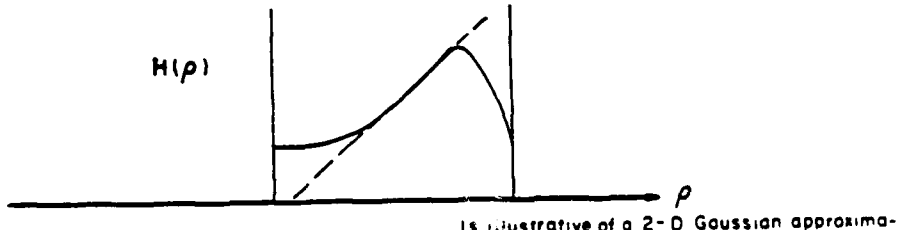

Is illustrative of a 2-D Gaussian approximation to a 2-D ellipsoidal contour of the ambiguity function of the linear FM waveform

$$H(\rho) \simeq \frac{e^{-\alpha\rho^2}}{I_0(\beta\rho^2)}$$

FIG. 2

IMAGING SYSTEM

STATEMENT OF GOVERNMENT INTEREST

The invention described herein may be manufactured and used by or for the Government of the United States of America for governmental purposes without the payment of any royalties thereon or therefor.

BACKGROUND OF THE INVENTION

This invention relates to a method and means for improving an imaging system. In greater particularity it is for a method and means for incorporating the operations of resolution enhancement and apriori information utilization simultaneously in the design of an improved imaging system. In still greater particularity it is to provide for an improved method and means for improving an imaging system that is adapted to imaging in a synthetic aperture radar, or in an inverse synthetic aperture radar, a radiometer, a sonar, an electromagnetic or acoustic tomographic system or a related system in which there is an interaction between the measurements that are being taken of physical phenomenon and the phenomenon which are being observed.

Recently an analogy has become recognized which exists between delay-doppler imaging-radar systems and tomographic systems used in clinical radiology. The analogy appears to hold the possibility of improving radar imaging because the use of matched filtering for noise suppression is suggested even by initial comparisons, and, more importantly because a line of thinking is emerging by which new mathematical models for the radar-imaging problem might be formulated and solved for improving processing. These new models account for dominant effects including noise. M. Bernfeld, in his article entitled "Chirp Doppler Radar" *Proceedings IEEE, Vol.* 72, No. 4 pp 540–541, April 1984, made a restricted form of this observation and the restricted form also appears in a different form in the work of D. Mensa, S. Halevy, and G. Wade in their article entitled "Coherent Doppler Tomography for Microwave Imaging" *Proceedings IEEE, Vol.* 71, No. 2 pp 254–261, February 1983. Both of these articles draw the analogy to a tomography system wherein the data available for processing are in the form of idealized, noise-free line-integrals through the object being imaged. This type of tomography system embraces a situation that is well approximated with X-ray tomography systems because X-ray sources can be highly collimated so as to form narrow X-ray beams of high intensity that are passed through the object being imaged. Although the analogy was articulated in these two articles, there is strong reason to believe that its applicability to practical radar/sonar signals of interest is limited because the ambiguity functions normally associated with such radar/sonar signals do not approximate line distributions in mass and thus do not permit the evaluation of line integrals of the scattering function. Two additional writings dealing with frequency-stepped, chirp-signals have discussions which clarify this limitation. M. Prickett, and C. Chen in "Principles of Inverse Synthetic Aperture Radar (ISAR) Imaging," *IEEE EASCON Record*, pp. 340–345, September 1980 and M. Prickett and D. Wehner in "Stepped Frequency Target Imaging", *Applications of Image Understanding and Spatial Processing to Radar Signals for Automatic Ship Classification Workshop*, New Orleans, La., February 1979 discuss side lobe structures and other features that cause a departure from idealized line-integrals and the fact that noise can be non-negligible in some radar-imaging situations. A solution was not evident, however. These articles are included in the Appendix for a reader's convenience.

Thus, there is a continuing need in the state-of-the-art for a method and means which may permit the removal of the restriction of noise-free line-integrals so that general magnitude squared ambiguity functions can be accommodated and the recognition of the effects of noise can be developed for improved imaging. In this discussion the ambiguity function is defined as the magnitude squared of the time-frequency autocorrelation or cross correlation function.

SUMMARY OF THE INVENTION

The present invention is directed to providing a means and method for improving the target imaging provided by a series of discrete data parameterized by a variable such as an angle θ in an imaging system which receives data representative of a physical phenomena and the pheonomena being observed and the interaction of data therebetween. Providing a plurality of discrete data inputs each for one of the series of discrete data enables a convolving-processing in parallel to generate two-dimensional preimage functions:

$$f_\theta(\tau,f)=\int\int \rho_\theta(\tau',f')w_\theta(\tau-\tau',f-f')d\tau'df'$$

where $f_\theta(\tau',f')$ as a function of θ,τ',f' is the set of available data and w_θ are chosen by the system designer. Summing the two-dimensional preimage functions enables a convolving the summed functions with a circularly symmetric function h where h is obtained from the equation:

$$d(\tau,f)=\int\int h(\tau-\tau',f-f')\rho(\tau',f')d\tau df.$$

where d is the desired response to a known distribution ρ. In particular if $\rho(\tau',f')$ is a two-dimensional delta function, then h is the point spread function of the imaging system.

A prime object of this invention is to improve the design of an imaging system.

Another object is to provide for an improved method and means for improving an imaging system relying on an interaction between the measurements taken of a physical phenomena and the phenomena which is being observed.

Still another object of the invention is to provide for an improved imaging system relying upon new processing algorithms implemented by associated circuitry that provide improved visualization of targets.

Another object is to provide for an improved method and means for imaging targets having specialized processing for real time implementations.

Yet still another object of the invention is to provide for an improved imaging system such as in a synthetic aperture radar, an inverse synthetic aperture radar, a sonar, an electrometric or acoustic tomographic system or related system having a target image provided by a series of data parameterized by a variable such as angle θ.

These and other objects of the invention will become more readily apparent from the ensuing specification and drawing when taken in conjunction with the appended claims.

BRIEF DESCRIPTION OF THE DRAWINGS

FIG. 1 is a schematic representation of a preferred form of the invention.

FIG. 2 is illustrative for a 2D Gaussian approximation of the 2D ellipsoidal contour of the ambiguity function of the linear FM waveform.

DESCRIPTION OF THE PREFERRED EMBODIMENTS

First, a mathematical analysis of radar imaging is presented and analogized to a related analysis concerning a tomographic imaging system. These two technological discussions are set forth to provide a thorough appreciation of the salient features of a specific embodiment of this inventive concept. It is of course understood that the analogies of these systems and a consequent improvement by the inclusion of this inventive concept are also applicable to imaging synthetic aperture radar, inverse synthetic aperture radar, radiometric systems, sonar systems or other devices in which there is an interaction between the measurements that are being taken of the physical phenomenon and the phenomenon which are being observed. More specifically this improvement can be incorporated in systems which enable the taking of a series of measurements not identically repeating the same measurements but paramaterized by a variable which is generally designated as an angle θ. This need not necessarily be a physical angle in the case of an inverse synthetic aperture radar but could be the angle made by the ambiguity function of the chirp waveform relative to the delay axis on each successive transmission and is the chirp rate of the actual signal transmitted. In the case of a radiometer it is the real angle in which the radiometer observes the scene of which it is trying to form an image.

In other words, this concept applies to a system in which there exists a free parameter called an angle θ and that a series of measurements is made, each one of these measurements at a different angle of $\theta_1, \ldots \theta_n$. It is recognized that each measurement may itself be a series of submeasurements in which the angle is held constant so as to improve the quality of the measurement at that angle. What is being described is the combination of these multiple measurements and a reconstruction algorithm which has the capability of providing high resolution and simultaneously the incorporation of apriori knowledge. For example, in conventional X-ray tomography an attenuation projection can be measured that is an integral of some physical property, a scattering cross-section is measured in the case of an inverse synthetic aperture radar and a voluminous flux projection is measured in the case of a radiometer. A set of integrals is available for these functions. The fundamental theorem forming the subject matter of this improvement is the radon inversion lemma which says that a Fourier transform of this observation of the one-dimensional projections is represented as a slice through the two-dimensional Fourier transform of the distribution that is trying to be measured. This, however, standing by itself is equivalent to having no additional information available and, therefore, the evaluation of the inverse radon transform tends to be numerically unstable and is equivalent to doing numerical differentiation.

However, addition apriori information often is available. For example, we know the range resolution in the case of an inverse synthetic aperture radar, or when cross-bearing fixes are provided in the case of a radiometer, they give an indication of the approximate range. This apriori information can be incorporated in precisely the same way that it is incorporated in the positron emission tomography that is referenced herein and discussed in greater detail below. That is to say, that instead of doing a back projection which is a transformation of a one-dimensional data field into a two-dimensional data field by spreading the one-dimensional data field everywhere parallel to itself into two-dimensions, the information is spread in a region determined by the available apriori knowledge. This apriori knowledge indicates a probability that the information is more likely to be known in one region than it is in another region and therefore it is not necessary to spread the information uniformly over lines in the two-dimensional plane by back projection. This operation is referred to with respect to positron emission tomography as "confidence weighting" but may be interpreted as being a weighting of the information according to whatever form of apriori knowledge that is available that indicates that the information is more likely to be encountered in one portion of the plane than uniformly along lines (back projection) in the plane.

Radar imaging has been typified and characterized by a number of parameters. These are discussed at length by H. L. Van Trees in his text "*Detection, Estimation, and Modulation Theory: Vol.* 3, John Wiley and Sons, New York, 1971. The parameter $\rho(\tau,f)$ is the target scattering-function which is the average reflectivity as a function of delay τ and doppler f, see pp. 448 of the Van Trees text. The parameter $a(\tau,f)$ denotes the ambiguity function of the transmitted radar-signal, (page 279 of Van Trees). In the absence of noise, the output $p(\tau,f)$ of a radar receiver consisting of a bandpass matched-filter (BPMF) matched to the transmitted radar signal) followed by a square-law envelope-detector (SLED) is the convolution of the target scattered function and the ambiguity function of the transmitted signal. Throughout this inventive concept, ambiguity function, $a(\tau,f)$ refers to the *magnitude squared* ambiguity function as elucidated in somewhat different notation in the Van Trees text. These expressions are set forth on pages 462 and 463 of the Van Trees text and form the basis for:

$$p(\tau,f)=\int\int \rho(\tau',f')a(\tau-\tau',f-f')d\tau'df'. \quad (1)$$

For the delay-doppler radar-imaging problem without noise, a sequence of target illuminations by chirp-FM signals is considered. Each of the chirp-FM signals has a different chirp rate. The effect of changing the chirp rate of a signal on its ambiguity function is to rotate the ambiguity function to an angle θ in the delay-doppler plane, (page 291 of Van Trees). This dependency is indicated in equation (1) by changing the notation:

$$p_\theta(\tau,f)=\int\int \rho(\tau',f')a_\theta(\tau-\tau',f-f')d\tau'df'+n(\tau,f) \quad (2)$$

where θ is determined by the chirp rate relative to the radar pulse without chirp-FM and $n(\tau,f)$ is an undesired, naturally occurring contaminating noise function which is to be minimized according to well established techniques. The noise-free radar-imaging problem arises in the observation of the output of the BPMF-SLED receiver, $p_\theta(\tau,f)$ for a sequence of target illuminations having different chirp-FM rates, $\theta=\theta_0, \theta_1, \ldots \theta_n$ and to determine the scattering function $\rho(\tau,f)$.

To elaborate, in the case of the chirp waveform, the angle is not the real angle as it would be in the case of trying to do a triangulation with a radiometer or doing the actual physical measurement in the positron emission tomograph. The chirp waveform angle is a valid parameter, however. It has been known in the art since the fundamental paper by Klauder in the Bell System Technical Journal in 1960 in that the response of a radar to a chirp waveform is parmeterized by a chirp rate number. This chirp rate number, the rate at which the frequency is changing, parameterizes the ambiguity function, that is, its ability to localize as a function of delay and doppler, which is inclined in the delay doppler plane at a physical angle proportional to the chirp rate, which is the mathematical parameter that describes how fast the chirp changes. Stated in another way, if the chirp does not change at all, the angle is 0 and then one has the ability to localize precisely in doppler because there is an equivalency to a continuous sample of a sinusoid and there is almost no ability to resolve as a function of delay. As the chirp rate is increased, range and doppler are coupled together so that a two-dimensional surface is defined which relates the ability of the waveform to resolve the target. By analogy to the usage for optical imating systems, the term "point spread function" can be used to describe this quantity since the ability of the radar to resolve a single point target is being described and is ambiguous in the sense that some of the targets at a near range will be received by the radar precisely the same way for their doppler as the targets at a larger range will be received with their doppler. That is, the target point gives rise to a response surface with a contour which is an ellipse whose major axis is along the line in range delay doppler space parameterized by the angle θ.

Recent developments in positron-emission tomographic imaging systems have a relation analogous to equation (2). In these tomographic systems a positron-emitting radionuclide is introduced inside a patient, and the resulting activity is observed externally with an array of scintillation detectors surrounding the patient in a planar-ring geometry. When a positron is produced in a radioactive decay, it annihilates with an electron producing two high energy photons that propagate in opposite directions along a line. In the first system employing positron emission, the line-of-flight of the two oppositely propagating photons is sensed for each detected event. The data attributed to these events are organized according to their propagation angle and processed with the same algorithms used in X-ray tomography. The result is an estimate of the two-dimensional spatial distribution of the radionuclide within the patient in the plane of the detector ring. Recent developments attributed to improvements in high-speed electronics and detector technology have made it feasible to measure the useful accuracy not only of the line-of-flight of annihilated photons but also their differential time-of-flight. As a consequence, in the absence of noise, the measurements are in the form of information of equation (2) with $\rho(\tau,f)$ being a two-dimensional activity distribution to be imaged and with $a_\theta(\tau,f)$ being the error density associated with measuring the location of an annihilation event. In this regard $\rho(\tau,f)$, $a_\theta(\tau,f)$, and $p_\theta(\tau,f)$ correspond to $\lambda(x)$, $p_\theta(x/\theta)$, and $\mu(n,\theta)$, respectively, where x and μ are two-dimensional vectors. These parameters and their applicability to positron emission tomography systems are explained in the article by D. L. Snyder, L. J. Thomas, Jr., and M. M. Ter-Pogossian entitled "A Mathematical Model for Positron Emission Tomography Systems Having Time-of-Flight Measurements" *IEEE Transactions on Nuclear Science, Vol. NS-28*, pp. 3575–3583, June 1981, see the appendix.

The noise-free imaging problem of emission tomography is to observe the line-of-flight and the time-of-flight of the sequence of detected annihilation photons, modeled on the average by $p_\theta(\tau,f)$ in equation (2) and to determine the two-dimensional activity distribution $\rho(\tau,f)$. Here, the parameter $a_\theta(\tau,f)$ is a known function determined by instrumentation errors and $p_\theta(\tau,f)$ is the number of detected events having a line-of-flight with angle θ and differential time-of-flight corresponding to position (τ,f) along the line-of-flight. In a recent experiment the data has been quantized to ninety-six angles ($\theta_i = 180i/96$, $i=0, 1, \ldots, 95$) and to 128-by-128 positions collected in an instrument being developed at Washington University and discussed by J. Blaine, D. Ficke, R. Hitchens, and T. Holmes in their article "Data Acquisition Aspects of Super-PETT," *IEEE Transactions on Nuclear Science Vol. NS-29*, pp. 544–547, February 1982, see the Appendix.

The error density $a_\theta(\tau,f)$ is determined by both the physical size of the crystals used in the scintillation detectors (resulting in about a 1-centimeter uncertainty transverse of the line-of-flight) and the timing resolution of the electronic circuitry used to measure the differential propogation-time (resulting in about a 7-centimeter spatial uncertainty along the line-of-flight). For present systems, this density is reasonably modeled by a two-dimensional, elliptically assymetric Gaussian-function having its major axis oriented with the line-of-flight and its minor axis oriented transversely to this.

For the radar-imaging problem this density corresponds to the ambiguity function of a radar pulse having an envelope that is a Gaussian function and an instantaneous frequency that is a linear function of time and the phase which is a quadratic function of time.

From the foregoing for an improved delay-doppler radar-imaging system certain assumptions must be made, the first of which is that the target is illuminated by a sequence of radar pulses each having a distinct FM-chirp rate corresponding to angles $\theta = \theta_0, \theta_1, \ldots, \theta_n$ spanning the range from 0°–180°. A BPMF-SLED receiver produces data $p_\theta(\tau,f)$ for $\theta_0, \theta_1, \ldots, \theta_n$ and quantized values of (τ,f). The problem that remains is to estimate the target scattering function $\rho(\tau,f)$ using the relationship stated in equation (2). For emission-tomography imaging when both time-of-flight and line-of-flight information are available, event data is provided which is representative of $p_\theta(\tau,f)$ at angles $\theta = \theta_0, \theta_1, \ldots, \theta_n$ spanning 0–180 and quantized to values of (τ,f). The measurement-error density $a_\theta(\tau,f)$ is known. The activity distribution $\rho(\tau,f)$ is to be estimated using the relatinship in equation (2). In both cases, the delay-doppler radar-imaging and the emission-tomography imaging, the activity distribution $\rho(\tau,f)$ need be estimated using the relationship expressed in equation (2).

A number of preliminary considerations must be examined and defined to allow a more thorough comprehension of the improvement of this inventive concept. Part of the solution for improving the radar, tomography, sonar, or radiometer image lies in developing an appropriate algorithm for suitable processing of an output signal from a known BPMF-SLED receiver. The algorithm is derived by applying statistical-estimation theory to a mathematical model that accounts for the

noise and other effects seen in an emission-tomography system having time-of-flight measurements. The algorithm for solving equation (2) above was proposed by D. L. Snyder et al in their article referenced above. This algorithm was evaluated in a later writing by Snyder "Some Noise Comparisons of Data-Collection Arrays for Emission Tomography-Systems Having Time-of-Flight Measurements" *IEEE Transactions on Nuclear Science, Vol. NS-29*, No. 1, pp. 1029–1033, February 1982 and by Politte and Snyder in the article "A Simulation Study of Design Choices in the Implementation of Time-of-Flight Reconstruction Algorithms" *Proceedings Workshop on Time-of-Flight Tomography*, Washington University, May 1982, published by the IEEE Computer Society, IEEE Catalog No. CH1791-3, please see these articles in the Appendix.

The noise was found to be Poisson distributed as might be expected because of the quantum nature of radioactivity decay, an effect well modeled by a Poisson process with intensity $\rho(\tau,f)$ proportional to the concentration of the radioactive source. It is argued in the earlier referenced D. L. Snyder et al article that the measured data (that is, line- and time-of-flight of annihilation photons) are also Poisson distributed, with the intensity being $p_\theta(\tau,f)$ in equation (2). Maximum-likelihood estimation is then used to estimate $\rho(\tau,f)$. An extension of this algorithm development is discussed in a later article by D. L. Snyder et al entitled "Image Reconstruction from List-Mode Data in an Emission Tomography System Having Time-of-Flight Measurements" *IEEE Transactions on Nuclear Science, Vol. NS-20*, No. 3, pp. 1843–1849, June 1983, see Appendix. The extended algorithm development is said to enable far more accurate reconstructions at the expense of greatly increased computation.

Neglecting the effects of noise and statistical fluctuations in the measurement data enable the expression of $p_\theta(\tau,f)$ as the measurement described above. The improved imaging system 10 for enhanced radar imaging, radiometer imaging, sonar imaging, and the like adapts itself to the established state-of-the-art and improves thereon, see FIG. 1. The output $p_\theta(\tau,f)$ of a BPMF-SLED receiver, schematically represented as memory 15, is three-dimensional because it is a function of the three idependent variables θ, τ, and f. The target image sought, $\rho(\tau,f)$ however, is two-dimensional. Thus, a three-dimensional to two-dimensional transformation of $p_\theta(\tau,f)$ is required as part of the improved processing.

The improved processing is accomplished in two steps. The first step is to form a two-dimensional "preimage array" 20. This is accomplished by convolving the data $p_\theta(\tau,f)$ obtained at each FM-chirp rate θ with a weighting function $w_\theta(\tau,f)$ and then summing the results over θ; that is we form the functions

$$f_\theta(\tau,f)=\int\int p_\theta(\tau',f')w_\theta(\tau-\tau',f-f')d\tau'df' \quad (3)$$

from which a two-dimensional preimage $f(\tau,f)$ is derived according to

$$f(\tau,f)=\int_0^\pi f_\theta(\tau,f)d\theta \cong \Sigma f_\theta(\tau,f). \quad (4)$$

The formation of this preimage corresponds to some extent with the back-projection step of the "unfiltered back-projection, post two-dimensional filtering" approach to idealize line-integral tomography. Examples of weighting functions that might be adapted are:

$$w_\theta(\tau,f)=(\delta\tau\delta f)^{-1}I_{\delta\tau}(\tau)I_{\delta f}(f) \quad (4a)$$

where,

$$I_{\delta\tau}(\tau)I_{\tau f}(f)=1, \ |\tau|\leq\delta\tau/2, \ |f|\leq\delta f/2=0, \text{ otherwise.} \quad (4b)$$

Here, $w_\theta(\tau,f)$ is unity for delays and dopplers in a small bin located at τ and f in the delay-doppler plane and is zero otherwise, independently of the sweep rate θ. In this case, $f_\theta(\tau,f)$ equals $p_\theta(\tau,f)$, and the preimage is

$$f(\tau,f)=\int_0^\pi p_\theta(\tau,f)d\theta \cong \Sigma_\theta p_\theta(\tau,f). \quad (4c)$$

This choice of $w_\theta(\tau,f)$ might be reasonable if the ambiguity function $a_\theta(\tau,f)$ is concentrated about the origin $(\tau,f)=(0,0)$, which requires a signal with a large time-bandwidth product. Then, $p_\theta(\tau,f)$ equals $\rho(\tau,f)$, and the preimage is obtained simply by post detection integration in each delay-doppler bin without further processing.

Give $w_\theta(\tau,f)$ a value of unity for values of delay and doppler within a narrow strip of width δ passing through the origin of the delay-doppler plane at angle θ and $w_\theta(\tau,f)$ a value of zero otherwise Then $f_\theta(\tau,f)$ is a strip integral, or line integral for δ small, through the data $p_\theta(\tau,f)$, which corresponds to unfiltered back-projection in tomography.

A confidence weighting function $w_\theta(\tau,f)=a_\theta(\tau,f)$ is used to form the preimage as suggested from the positron-emission tomography experience. This corresponds to taking the value of the BPMF-SLED signal $p_\theta(\tau,f)$ shown in the drawings as coming from measurement memories 15 at each value of delay and doppler $p_{\theta 1}(\tau,f)\ldots p_{\theta 96}(\tau,f)$ and distributing the values over the delay doppler plane according to the ambiguity function $a_\theta(\tau,f)$. This approach is the one now used routinely in emission-tomography systems having time-of-flight data. If the mathematical development of the cited Snyder et al paper on mathematical modeling carries over the radar-imaging problem, the choice of the weighting function is motivated by noting that the resulting $f_\theta(\tau,f)$ is the maximum-likelihood estimate of the delay-doppler reflectance in the target that led to the measurement $p_\theta(\tau,f)$ assuming apriori that $\rho(\tau,f)$ is uniform.

The second processing step in the imaging approach relies on the summing of the preimage outputs in a summer 25 and the deriving of a target image from the preimage in a convolver 30. Such a target image resolution is provided within a resolution function $h(\tau,f)$, which defines a "desired image" according to

$$d(\tau,f)=\int\int h(\tau-\tau',f-f')\rho(\tau',f')d\tau df. \quad (4d)$$

It has been found that including such a resolution function is important in processing emission-tomography data as a way to trade off resolution and smoothing for noise suppression. A narrow two-dimensional, circularly symmetric Gaussian resolution-filter is used as convolver 30. Let $\hat{d}(\tau,f)$ denote the estimate of $d(\tau,f)$ obtained by processing the preimage $f(\tau,f)$. Also let $\hat{D}(u,v)$ and $F(u,v)$ denote the two-dimensional Fourier transforms of $\hat{d}(\tau,f)$ and $f(\tau,f)$, respectively. Thus:

$$\hat{D}(u,v)=H(u,v)F(u,v)/G(u,v). \quad (5)$$

where H(u,v) (see FIG. 2) is the transform of $h(\tau,f)$ and G(u,v) is the transform of the function $g(\tau,f)$ defined according to

$$g(\tau,f) = (1/\pi) \int_0^{\pi} a_\theta(\tau,f) w_\theta(\tau,f) d\theta. \quad (6)$$

FIG. 2 is illustrative for the 2D Gaussian approximation for the 2D ellipsoidal contour of the ambiguity function of the linear FM waveform. This required filter function is provided for a general 2D contour in accordance with established techniques.

The image $d(\tau,f)$ is obtained from $\hat{D}(u,v)$ by a two-dimensional, inverse Fourier transformation. The functions $g(\tau,f)$ and G(u,v) are precomputable since they depend only on the ambiguity function and the weighting function used to form the preimage and not on the measured data.

For the choice of the weighting function:

$$w_\theta(\tau,f) = a_\theta(\tau,f). \quad (6a)$$

the function $g(\tau,f)$ is the average over θ of the square of the ambiguity function $a_\theta(\tau,f)$ is a two-dimensional asymmetric Gaussian function, and $g(\tau,f)$ is a Bessel function. The derivation does not require that $a_\theta(\tau,f)$ be Gaussian, but $g(\tau,f)$ will usually need to be evaluated numerically for practical ambiguity functions.

The processing thusly described lends itself to the radar-imaging enhancement and is motivated by the processing derived from a mathematical model for the emission-tomography imaging problem. The end result is an improved imaging for radar doppler, radiometric sonar and the like information gathering systems.

The architecture suggested by the algorithm defined by equation (3) through (6) above is similar to that discussed in a later article by D. L. Snyder entitled "Algorithms and Architectures for Statistical Image Processing in Emission Tomography" *Real Time Signal Processing VII. Vol.* 495, Society of Photo-Optical Instrumentation Engineers, pp. 109–111, 1984, see the Appendix. Data acquired for each doppler rate can be processed in parallel and then combined to form $f(\tau,f)$ according to equation (4) and the processing in equation (3) required for each doppler rate can be pipelined. The processing implemented in current emission-tomographs is performed in the spatial rather than the Fourier domain. The algorithm has been implemented by a computer, for example, a Perkin-Elmer 3242 computer with a floating point processor but no array processor. Two convolutions and a division are required at each stage for each of the data gatering angles. Simultaneous processing can be performed and pipelined for each angle.

Obviously many modifications and variations of the present invention are possible in the light of the above teachings such as substituting magnitude in place of magnitude squared. It is therefore to be understood that within the scope of the appended claims the invention may be practiced otherwise than as specifically described.

APPENDIX

List of Patents, Publications & Information

I. "Algorithms and Architectures for Statistical Image Processing in Emission in Tomography" by D. L. Snyder
pages 109–111, 1984
Real Time Signal Processing VII. Vol. 495.
Society of Photo-Optical Instrumentation Engineers

II. "Data Acquisition Aspects of Super-PETT".
by J. Blaine et al.
IEEE Trans. on Nuclear Science.
Vol. NS-29, pages 544–547. February 1982

III. "A Mathematical Model for Positron Emission Tomography Systems Having Time-of-Flight Measurements".
by D. L. Snyder et al.
IEEE Trans. on Nuclear Science.
Vol. NS-28, pages 3575–3583. June 1981

IV. "Some Noise Comparison of Data-Collection Arrays for Emission Tomography-Systems Having Time-of-Flight Measurements".
by D. L. Snyder
IEEE Trans. on Nuclear Science.
Vol. NS-29, pages 1029–1033. February 1982

V. "Image Reconstruction from List-Mode Data in an Emission Tomography System Having Time-of-Flight Measurements"
by D. L. Snyder et al.
IEEE Trans. on Nuclear Science.
Vol. NS. 20, No. 3,
pages 1843–1849. June 1983

VI. "CHIRP Doppler Radar".
by M. Bernfeld.
Proc. IEEE.
Vol. 72, No. 4, pages 540–541. April 1984

VII. "Coherent Doppler Tomography for Microwave Imaging".
by D. L. Mensa et al.
Proc. IEEE, Vol. 71, No. 2,
pages 254–261. February 1983

VIII. "Stepped Frequency Radar Target Imaging".
by M. J. Prickett et al.
(private correspondence)

IX. "Principles of Inverse Synthetic Aperture Radar (ISAR) Imaging".
by M. J. Prickett et al.
IEEE EASCON Record.
pages 340–345. September 1980

What is claimed is:

1. An apparatus for improving the target provided by a series of discrete target image data signals parameterized by a variable such as an angle θ comprising:

means for providing a plurality of target image data input signals $p_\theta(\tau f)$ each for one of the series of discrete target image data signals;

means coupled to a separate input providing means for processing the target image data input signals in total to generate separate two-dimensional preimage functions $f(\tau,f)$;

means for summing the two-dimensional preimage functions;

means coupled to summing means for convolving the summed preimage functions with a response function to form an improved target image signal according to the equation

$$d(\tau,f) = \int\int h(\tau-\tau',f-f')p(\tau',f')d\tau df$$

that has equivalence as

$$D(u,v) = H(u,v)F(u,v)/G(u,v)$$

in Fourier transform notation where H(u,v) is the Fourier transform of $h(\tau,f)$; and

means coupled to the convolving means for controlling the display of an enhanced image in response to the improved target image signal.

2. An apparatus according to claim 1 in which each of the target image data input signal providing means is fabricated to provide a separate one of the target image data input signals from a separate one of the series of discrete target image data signals to be characterized by the function:

$$p_\theta(\tau,f)=\int\int p(\tau',f')a_\theta(\tau-\tau',f-f')d\tau'df'.$$

over θ angle $=\theta_0 \ldots \theta_n$.

3. An apparatus according to claim 2 in which each of processing means is fabricated to convolve the data $p_{\theta 1}(\tau,f) \ldots p_{\theta n}(\tau,f)$ with a confidence weighing function $w_\theta(\tau,f)$ to form the functions:

$$f_\theta(\tau,f)=\int\int p_\theta(\tau',f')w_\theta(\tau-\tau',f-f')d\tau'df'.$$

and the summing means sums over the angle θ to obtain the summed two-dimensional preimage function of:

$$f(\tau,f)=\int_0^\pi f_\theta(\tau,f)d\theta$$

which optionally is expressed as the approximate expression

$$f(\tau,f)\cong\Sigma f_\theta(\tau,f).$$

4. An apparatus according to claim 3 in which the convolving means is a two-dimensional, circularly symmetrical Gaussian resolution-filter whose impulse response is the solution computed by a two-dimensional, inverse Fourier transformation expressed as

$$g(\tau,f)=(1/\pi)\int_0^\pi a_\theta(\tau,f)w_\theta(\tau,f)d\theta$$

that has equivalence as a two-dimensional, circularly symmetrical Gaussian resolution-filter which satisfies the equation:

$$\hat{D}(u,v)=H(u,v)/F(u,v)/G(u,v)$$

where G(u,v) is the Fourier transform of $g(\tau,f)$.

5. A method of improving a target image from a series of discrete target image data signals parameterized by a variable such as an angle θ comprising:

providing a plurality of discrete target image data input signals each for one of the series of discrete target image data signals and each target image data input signals expressed as:

$$p_\theta(\tau,f)=\int\int p(\tau',f')a_\theta(\tau-\tau',f-f')d\tau'df'+n(\tau,f)$$

where $n(\tau,f)$ is an undesired naturally occurring noise function over θ angle $=\theta_0 \ldots \theta_n$;

processing in total the plurality of series of discrete target image data input signals to generate two-dimensional preimage functions $f_\theta(\tau,f)$;

summing the plurality of two-dimensional preimage functions; convolving the summed plurality of two-dimensional preimage functions into an improved target image signal corresponding to the function

$$d(\tau,f)=\int\int h(\tau-\tau',f-f')p(\tau',f')d\tau df$$

and

controlling the display of the improved target image signal to provide an improved target image on a viewing screen.

6. A method according to claim 5 in which the step of processing convolves each discrete target image data input signals $p_\theta(\tau,f)$ with a weighting function $w_\theta(\tau,f)$ to be expressed as:

$$f_\theta(\tau,f)=\int\int p_\theta(\tau',f')w_\theta(\tau-\tau',f-f')d\tau'df'.$$

to each obtain the two-dimensional preimage function of:

$$f(\tau,f)=\int_0^\pi f_\theta(\tau,f)d\theta$$

for angle $\theta=\theta_0 \ldots \theta_n$ which optionally is expressed as the approximate expression:

$$f(\tau,f)\cong\Sigma f_\theta(\tau,f).$$

7. A method according to claim 6 in which the step of convolving with a circularly symmetric response function relies on a two-dimensional circularly symmetrical Gaussian resolution-filter computed by a two-dimensional inverse Fourier transformation expressed as:

$$g(\tau,f)=(1/\pi)\int_0^\pi a_\theta(\tau,f)w_\theta(\tau,f)d\theta$$

that has an equivalence as a two-dimensional, circularly symmetrical Gaussian resolution-filter which satisfies the equation:

$$\hat{D}(u,v)=H(u,v)/F(u,v)/G(u,v)$$

where G(u,v) is the Fourier transform of $g(\tau,f)$.

* * * * *